Improving combustion chamber and pipe components of the European Space Propulsion System Simulation (ESPSS) library with AUSM scheme

Marco Leonardi*[1], Francesco Nasuti†[1], Francesco Di Matteo‡[2], Johan Steelant§[2], Jòse Francisco Moral¶[3], and Javier Vila Vacas‖[3]

[1]*University of Rome "La Sapienza", Dip. Ingegneria Meccanica e Aerospaziale, Rome, Italy*
[2]*ESA-ESTEC, Aerothermodynamic & Propulsion Analysis Section, Noordwijk, The Netherlands*
[3]*Empresarios Agrupados, Madrid, Spain*

Abstract

So far, the formulation of the ESPSS library included two schemes for the computation of the numerical fluxes: the donor-cell (centred) and the Roe scheme. The Roe splitting has been commonly accepted as one of the most accurate techniques available today. It is less dissipative than the centred scheme and then is preferable in some applications, however the related drawback is represented by an increase in the computational cost. Additionally, the Roe scheme cannot be extended to a different set of equations without changing the entire structure of the scheme itself. Since one of the key features of the ESPSS library is the flexibility, it is of paramount importance to include a scheme that, while being less dissipative than the centred scheme, can be easily extended to different set of equations. The AUSM scheme was originally devised as a simple scheme able to compete in accuracy with the Roe scheme. Subsequent modifications led to a robust scheme able to deal with a complete series of fluxes, thus making the AUSM an appealing alternative for the ESPSS library. We included the AUSM scheme in the ESPSS library, extending its original formulation to both multi-species and two-phase flows, thus improving the combustion chamber and the pipe components. In the present paper the implementation is detailed along with the needed validation tests, and the new components is applied to analyse cases of practical interest.

1 Introduction

When dealing with an engineering tool it is necessary to reduce the computational time to allow for fast computations. In the present paper we update the EcosimPro components included in both the FLUID_FLOW_1D and the COMB_CHAMBERS libraries of ESPSS [1] by means of a scheme for the computation of the inviscid fluxes. Before the work here performed the libraries were equipped with two schemes: the donor cell and the Roe scheme. The former scheme gained rapidly success among the EcosimPro community as its simple formulation relies on a staggered grid approach that matches almost perfectly with the resistive-capacitive building logic of the software. However, it is characterised by a considerable amount of dissipation that on one hand ensures a rather robust behaviour but on other may bring to some inaccuracies when simulating specific transient phases. Therefore, the Roe scheme was included beside the donor cell scheme to enable for more accurate transient simulations. However, the Roe scheme could be limiting for two reasons: it may bring to extremely long computational times when strong transient phases are simulated and it cannot be extended to different set of equations since it relies on the eigen-structure of the set of equations to be solved. In this frame we decided to include in the aforementioned libraries the AUSM+_up [2] scheme. The advantage of the scheme is twofold: (i) it allows for faster computations when compared to similar schemes and (ii) it can be extended to different set of equations since the interface fluxes are reconstructed in such a way that does not need any information on the eigen-structure of the equations.

2 Physical and Mathematical Model

The AUSM scheme has been implemented for two set of quasi-one-dimensional governing equations, namely: the Homogeneous Equilibrium Model (HEM) and the Euler equations for multi-species flow. The former model is the one implemented to describe the two-phase flow evolution in the FLUID_FLOW_1D library whereas the latter is employed to describe the evolution of the gases inside the combustion

*Ph.D, marco.leonardi@uniroma1.it
†Associate Professor, francesco.nasuti@uniroma1.it
‡Ph.D, Propulsion Engineer, francesco.di.matteo@esa.int
§Ph.D, Propulsion and Aerothermodynamic Engineer, johan.steelant@esa.int
¶frj@empre.es
‖jvv@empre.es

chamber components included in the COMB_CHAMBERS library. In the next sections we give a description of the AUSM scheme beside its implementation details for both models.

2.1 Homogeneous Equilibrium Model

The **H**omogeneous **E**quilibrium **M**odel (HEM), that is used within Ecosimpro, is a simple model to simulate the two-phase flow. Thanks to the hypothesis of flow in equilibrium it brings to a set of equations whose structure is close to the Euler equations and, more importantly, that are unconditionally hyperbolic. This is of course an attractive feature, because it gives a complete set of eigenvalues and eigenvectors and just four equations to be solved since both phases have the same velocity, pressure and temperature. The two-phase fluid can be either a simplified liquid, or a real fluid. The governing equations consider one continuity equation for the non-condensable perfect gas, one for the non-condensable perfect gas diluted in the liquid phase, one for the overall mixture, one momentum equation and one energy equation for the overall mixture. The set is completed by "N" equations one for each of the chemical species convected in the pipe. These latter continuity equations are needed when the pipe is located downstream of a component in which reactions take place, e.g. pre-burner and gas generator, and the convection of the gaseous burned species must be taken into account. It is worth noticing that both the non condensable gas and the two-phase fluid can be a real fluid whose properties are retrieved from a dedicated database. Different flow mixture configurations are possible, e.g. pure liquid, liquid and vapour, vapour and non-condensable. Therefore, flow properties must be calculated according to the mixture state and proper mixing rules have to be adopted. Details on calculation of the mixture properties can be found in the ESPSS reference manual [1]. The complete set of equations is:

$$\frac{\partial \boldsymbol{u}}{\partial t} + \frac{\partial \boldsymbol{f}(\boldsymbol{u})}{\partial x} = \boldsymbol{S}(\boldsymbol{u}) \tag{1}$$

with

$$\boldsymbol{u} = A \begin{pmatrix} \rho \\ \rho x_{nc} \\ \rho x_{nc}^{d} \\ \rho x_{chem,1} \\ \rho x_{chem,2} \\ \vdots \\ \rho x_{chem,N} \\ \rho u \\ \rho E \end{pmatrix} \quad \boldsymbol{f}(\boldsymbol{u}) = A \begin{pmatrix} \rho u \\ \rho x_{nc} u \\ \rho x_{nc}^{d} u - D\dfrac{\partial x_{nc}^{d}}{\partial x} \\ \rho x_{chem,1} u \\ \rho x_{chem,2} u \\ \vdots \\ \rho x_{chem,N} u \\ \rho u^2 + p \\ \rho u H \end{pmatrix}$$

$$\boldsymbol{S}(\boldsymbol{u}) = \begin{pmatrix} -\rho A \kappa_w \dfrac{\partial p}{\partial t} \\ -\rho x_{nc} A \kappa_w \dfrac{\partial p}{\partial t} + V(R_d - R_a) \\ -\rho x_{nc}^{d} A \kappa_w \dfrac{\partial p}{\partial t} - V(R_d - R_a) \\ -\rho x_{chem,1} A \kappa_w \dfrac{\partial p}{\partial t} \\ -\rho x_{chem,2} A \kappa_w \dfrac{\partial p}{\partial t} \\ \vdots \\ -\rho x_{chem,N} A \kappa_w \dfrac{\partial p}{\partial t} \\ -\dfrac{\partial q_n}{\partial x} + p\frac{dA}{dx} - 0.5\dfrac{\partial \xi}{\partial x}\rho u|u|A - \rho g A \\ \dfrac{dq_w}{dx} - \rho u A \kappa_w \dfrac{\partial p}{\partial t} + \rho g u A \end{pmatrix} \tag{2}$$

where "N" is the total number of chemical species, q_n an artificial dissipation term and, if no specification is made, the variables involved in the equations are those of the overall (two-phase + non-condensable gases) mixture. The source terms in the system Eq. (2) are related to different effects taking part in the quasi-one-dimensional two-phase:

- $\rho x_{nc,chem} A \kappa_w \dfrac{\partial p}{\partial t}$ models the compressibility due to the volume change related to wall effects
- $V(R_d - R_a)$ is the exchange term related to the effects of absorption and desorption of the non-condensable gas into the liquid phase, where R_d and R_a are calculated with dedicated correlations
- $0.5\dfrac{\partial \xi}{\partial x}\rho u|u|A$ is the distributed friction
- $\rho g A$ models the gravity effects on the mixture, that become effective only if the pipe is in a non-horizontal portion
- $p\frac{dA}{dx}$ is related to the quasi-one-dimensional formulation
- q_w is the heat exchanged with the walls
- $\rho g u A$ and $\rho x_{nc,chem} u A \kappa_w \dfrac{\partial p}{\partial t}$ are the work associated to gravity and compressibility.

As for the mixture properties, the reader is referred to the ESPSS reference manual [1] also for the definition of coefficients implied in the listed source terms. The first step in the formulation of the AUSM scheme is to recognise the convection and the acoustic waves as two physically distinct processes. Therefore inviscid flux as in Eq. (2) can be written as the sum of the convective and the pressure terms

$$\boldsymbol{f}(\boldsymbol{u}) = \boldsymbol{f}^{c}(\boldsymbol{u}) + \boldsymbol{P} \tag{3}$$

where the convective fluxes and the pressure term vary according to the original set of equations.

It is common to all the AUSM schemes to express the convective flux $\boldsymbol{f}^{c}(\boldsymbol{u})$ in terms of a common scalar mass flux and

passive scalar quantities. This approach can be retrieved also in the HEM formulation, since both phases are supposed to travel at the same velocity

$$\boldsymbol{f}^c(\boldsymbol{u}) = \dot{m} \begin{pmatrix} 1 \\ x^{nc} \\ u \\ H \end{pmatrix}, \quad \boldsymbol{P} = \begin{pmatrix} 0 \\ 0 \\ p \\ 0 \end{pmatrix} \tag{4}$$

where the pressure flux $\boldsymbol{P}$ contains just the pressure term. It is now possible to write a numerical flux at each cell interface, in terms of the common mass flux

$$\boldsymbol{f}_{1/2} = \dot{m}_{1/2} \boldsymbol{\Psi}_{L/R} + \boldsymbol{P}_{1/2} \tag{5}$$

where $\boldsymbol{\Psi}_{L/R}$ is determined in a simple upwind fashion

$$\boldsymbol{\Psi}_{L/R} = \begin{cases} \boldsymbol{\Psi}_L & \text{if} \quad \dot{m}_{1/2} \geq 0 \\ \boldsymbol{\Psi}_R & \text{otherwise} \end{cases} \tag{6}$$

Clearly the main task is now to define the mass and the pressure fluxes. The definition in Eq. (6) is common to all the AUSM family schemes and the way in which the flux are treated is the key that characterises each formulation. The AUSM+up scheme was inspired from the needs to suppress some deficiencies observed with the previous AUSM and AUSM+ [2]. The most notable deficiencies are related with some pressure oscillations observed along the grid direction in which a small velocity component is registered. To serve the scope some diffusion terms are added to the original formulation.

At each cell interface we can write the mass flux as:

$$\dot{m}_{1/2} = u_{1/2}\rho_{1/2} = a_{1/2}M_{1/2}\rho_{1/2} \tag{7}$$

where $u_{1/2}$ is the convective velocity and $\rho_{1/2}$ the density convected by $u_{1/2}$. The velocity can be expressed in terms of polynomial functions of eigenvalues associated with the non-linear fields, so that the upwind switching can be automatically formulated at the sonic condition. Thus, the mass flux is expressed as :

$$\dot{m}_{1/2} = a_{1/2}M_{1/2} \begin{cases} \rho_L & \text{if} \quad M_{1/2} \geq 0 \\ \rho_R & \text{otherwise} \end{cases} \tag{8}$$

Different approaches have been proposed to treat the interface speed of sound $a_{1/2}$ [3]. We here adopt an averaged form of the numerical speed [4]:

$$a_{1/2} = \sqrt{\frac{\rho_L a_L^2 + \rho_R a_R^2}{\rho_R + \rho_R}} \tag{9}$$

where the left and right speed of sound is found from a simple average based on the void fraction

$$a_{L,R} = \left(\rho \left(\frac{\alpha}{\rho_g {a_g}^2} + \frac{1-\alpha}{\rho_l a_l^2} \right) \right)^{-\frac{1}{2}} \tag{10}$$

and void fraction is defined as

$$\alpha = \frac{\rho - \rho_{liq}}{\rho_{liq} - \rho_{vap}}$$

From the numerical speed of sound a left and a right Mach numbers can be defined accordingly

$$M_{L/R} = \frac{u_{L/R}}{a_{1/2}} \tag{11}$$

The interface Mach number can now be expressed in terms of M_L and M_R as:

$$M_{1/2} = \mathcal{M}^+_{(m)}(M_L) + \mathcal{M}^-_{(m)}(M_R) + M_p \tag{12}$$

The split Mach numbers $\mathcal{M}^{\pm}_{(m)}$ are polynomial functions of degree m (=1, 2, 4):

$$\mathcal{M}^+_{(1)}(M) = \frac{1}{2}(M \pm |M|) \tag{13}$$

$$\mathcal{M}^+_{(2)}(M) = \pm\frac{1}{4}(M \pm 1)^2 \tag{14}$$

and

$$\mathcal{M}^+_{(4)}(M) = \begin{cases} \mathcal{M}^{\pm}_{(1)} & \text{if} \quad |M| \geq 1 \\ \mathcal{M}^{\pm}_{(2)}(1 \mp 16\beta\mathcal{M}^{\mp}_{(2)}) & \text{otherwise} \end{cases} \tag{15}$$

The pressure diffusion term M_p, introduced to enhance calculations of low Mach numbers or multi-phase flow, is defined as:

$$M_p = -K_p \max(1 - \sigma\bar{M}^2, 0)\, \frac{p_R - p_L}{\rho_{1/2} a_{1/2}^2}, \qquad \sigma \leq 1 \tag{16}$$

$$\rho_{1/2} = \frac{\rho_L + \rho_R}{2}$$

with $0 \leq K_p \leq 1$.

The factor $\max(1 - \sigma\bar{M}^2, 0)$ is activated only in the region of $M^2 \leq \frac{1}{\sigma}$ with $\sigma \leq 1$. The second term on the right hand side of Eq. (5) is formulated in all the AUSM-family schemes as:

$$p_{1/2} = \mathcal{P}^+_{(n)}(M_L)p_L + \mathcal{P}^-_{(n)}(M_R)p_R \tag{17}$$

where $n = 1, 3, 5$ corresponds to the degree of the polynomials $\mathcal{P}^{\pm}$. The fifth degree polynomials are preferred because they are found to give a more accurate solution. They are also expressed in terms of the split Mach numbers functions in Eqs. (13) and (14)

$$\mathcal{P}^{\pm}_{(5)}(M) = \begin{cases} \frac{1}{M}\mathcal{M}^{\pm}_{(1)} & \text{if} \quad |M| \geq 1 \\ \mathcal{M}^{\pm}_{(2)}[(\pm 2 - M) \mp 16\alpha M \mathcal{M}^{\mp}_{(2)}] & \text{otherwise} \end{cases} \tag{18}$$

The pair α, β is commonly set to $(3/16, 1/8)$ [5]. The above expression is then modified by adding a velocity diffusion term similar to the one introduced for the interface Mach number in Eq. (12):

$$p_{1/2} = \mathcal{P}^+_{(5)}(M_L)p_L + \mathcal{P}^-_{(5)}(M_R)p_R + p_u \tag{19}$$

where

$$p_u = -K_u \mathcal{P}^+_{(n)}(M_L)\mathcal{P}^-_{(n)}(M_R)(\rho_L + \rho_R)a_{1/2}(u_R - u_L) \tag{20}$$

and the coefficient $0 \leq K_u \leq 1$. It is worth to notice that this velocity diffusion term is an approximation of the characteristic relations $dp \pm \rho a du = 0$ to yield,

$$p_{1/2} = \frac{1}{2}(p_L + p_R) - \frac{1}{2}(pa)_{1/2}(u_R - u_L) \tag{21}$$

for M_L, $M_r \leq 1$. The coefficient $\mathcal{P}^+_{(n)}(M_L)\mathcal{P}^-_{(n)}(M_R)$ simply switches off p_u as the flow becomes supersonic, resulting in a one sided up-winding. Several members of the AUSM family also have a similar term [6, 7, 8].
It is noteworthy that the parameter σ has an influence on the solution near the sonic point, in particular its action is to smooth the solution as it becomes smaller. Please note that this parameter influences the solution only in the supersonic region where $1 \leq M^2 \leq \frac{1}{\sigma}$ with $0 \leq \sigma \leq 1$. It has been noticed [3] that the lower bound for σ may be set by a requirement that the exact shock capturing property is preserved, namely

$$M_P = 0 \; \forall \; \bar{M} \geq 1 \quad \Rightarrow \quad 1 - \sigma^* \bar{M}^2 = 0, \; \sigma^* \leq \sigma \leq 1 \tag{22}$$

If $\bar{M}^2 = (M_L^2 + M_R^2)/2$ and using the well known Prandtl relation one gets the analytical expression for σ^*

$$\sigma^* = \frac{2}{1 + (M_L a_L / a_L^*)^4} \tag{23}$$

If the region activated by the factor $\max(1 - \sigma \bar{M}^2, 0)$ is to be narrowed, then a value close to one should be chosen.

2.2 Multi-species model

In the combustion chamber component the set of equations takes a different form with respect to the HEM model. It takes into account the evolution of a multi species gaseous flow with a simple model for the vaporisation of the liquid droplet. The set of equations can be expressed as in section section 2.1, with:

$$\boldsymbol{u} = A\rho_{mix} \begin{pmatrix} 1 \\ \vdots \\ x_k \\ \vdots \\ x_{red} \\ x_{oxy} \\ x_{pw} \\ x_{nc} \\ x_{bu} \\ u \\ E \end{pmatrix}$$

$$\boldsymbol{f}(\boldsymbol{u}) = A\rho_{mix} \begin{pmatrix} uA \\ \vdots \\ x_k uA \\ \vdots \\ x_{red} uA \\ x_{oxy} uA \\ x_{pw} uA \\ x_{nc} uA \\ x_{bu} uA \\ (u^2 + p/\rho_{mix})A \\ uHA \end{pmatrix} \quad \boldsymbol{S}(\boldsymbol{u}) = \begin{pmatrix} \vdots \\ Sm_k \\ \vdots \\ p\frac{dA}{dx} \\ \frac{dq_w}{dx} \end{pmatrix} \tag{24}$$

where Sm_k is the source term related to the production or consumption of the species k and the other terms have the same meaning of Eq. (2). In this case the convective part of the AUSM scheme in Eq. (4) is rewritten in accordance to the set of equations:

$$\boldsymbol{f}^c(\boldsymbol{u}) = \dot{m} \begin{pmatrix} 1 \\ \vdots \\ x_k \\ \vdots \\ x_{red} \\ x_{oxy} \\ x_{pw} \\ x_{nc} \\ x_{bu} \\ u \\ H \end{pmatrix} \tag{25}$$

The only difference with respect to the up-winding processes detailed in 2.1 is the interface speed of sound, that in this case is defined as a function of the left and right stagnation enthalpies:

$$a_{1/2} = f(Ho_L, Ho_R) \tag{26}$$

3 Validations and applications

The AUSM scheme is here validated through three tests. The first two are devoted to demonstrate the capabilities of the solver when applied to the HEM set of equations, thus involving tube components taken from the FLUID_FLOW_1D library. The third test involves the simulation of a complete gas generator engine in order to show the capabilities of the solver when applied to the combustion chamber components taken from COMB_CHAMBERS library.

3.1 Tube Component

The first part of the validation procedure is devoted to obtain steady state solutions of flow configurations for which an analytical solution can be found. This part of the validation is based on both subsonic and supersonic configurations for Fanno flow type in the tube component. The second part of

the validation procedure is instead devoted to tests embracing some typical transient phases of LREs feeding systems characterised by the presence of a two-phase mixture. In particular, an isolated branch of a feeding system will be investigated to reproduce water hammer effects, during which the liquid propellant is flown into a line filled with a gas and closed on one end. Therefore, the feed line undergoes high pressure peak cycles located at the dead-end of the pipe.

3.1.1 Steady state test case: Fanno flow

The Fanno test case consists of a flow in adiabatic conditions where the fluid evolution is due to the presence of friction effects. The pipe in which the fluid flows is one dimensional, hence no cross section variations are imposed, and the flow is considered in steady state conditions. Under these assumptions an analytic solution can be retrieved and compared to the results obtained with the ESPSS component. In case of subsonic inlet conditions the flow accelerates throughout the pipe and could reach a maximum velocity of $M = 1$. When the maximum speed is reached the flow is in choked conditions and cannot accelerate any further. If supersonic inlet conditions are imposed the flow decelerates along the pipe and, for high exit pressures and pipe length greater than the critical length, a shock moves upstream in the pipe causing the flow to decelerate to subsonic conditions. The three flow configurations will be tested hereafter, considering air flowing in a straight tube whose characteristic dimensions and numerical configurations are reported in Table 1. The set up of the model is based on a simple pipe with specific initial and boundary conditions, as shown in Fig. 1.

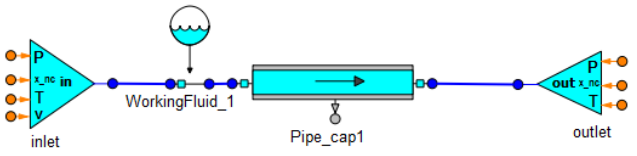

Figure 1: Fanno flow test case EcosimPro schematic

Geometry	
nodes	200
diameter [m]	0.043701937
roughness [m]	$5e^{-5}$
Numeric	
order	third
k_f	1
reconstructed_variable	conservative
Isent_Correl	TRUE

Table 1: Pipe_cap1 properties for Fanno flow test cases in Fig. 1

The initial and boundary conditions are reported in Table 2. Walls are not considered for this test, hence the tube component only models the flow evolution in a pipe with assigned friction. For both flow types different cases have been investigated, each of these is featuring a different length of the tube and a different outlet pressure. In particular these two parameters are changed to analyse the response of the pipe when the critical conditions are reached. The critical conditions for these configurations are characterised by a pipe length of $L = 1.2$ m and an outlet pressure $P = 250000$ Pa. The results obtained with the AUSM scheme are compared in Figs. 2 to 4 against the analytical solutions and those obtained with the Roe scheme. Both orders are employed with a third order accurate spatial reconstruction. In both subsonic and supersonic test cases a satisfactory matching between the analytical solution and the ESPSS solutions is reached. The AUSM scheme can reproduce the analytical solution with a high level of accuracy. The position of the shock is well de-

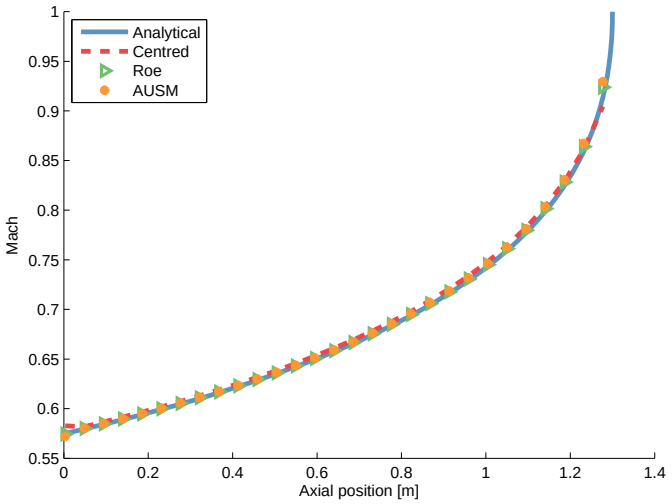

Figure 2: Fanno flow: subsonic tst case comparison of centred, Roe and AUSM scheme

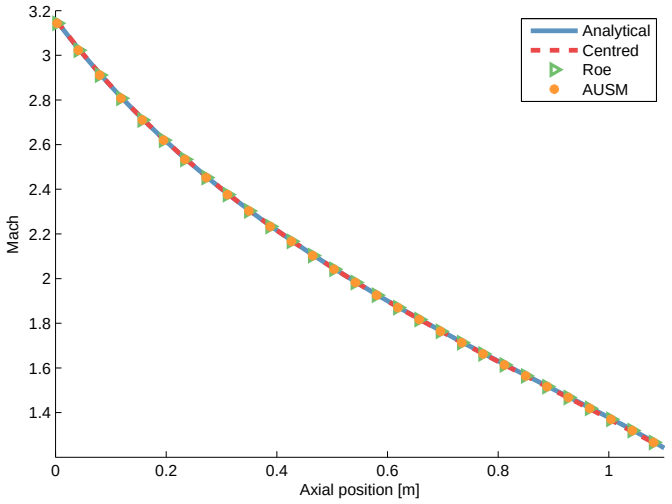

Figure 3: Fanno flow: supersonic test case comparison of centred, Roe and AUSM scheme

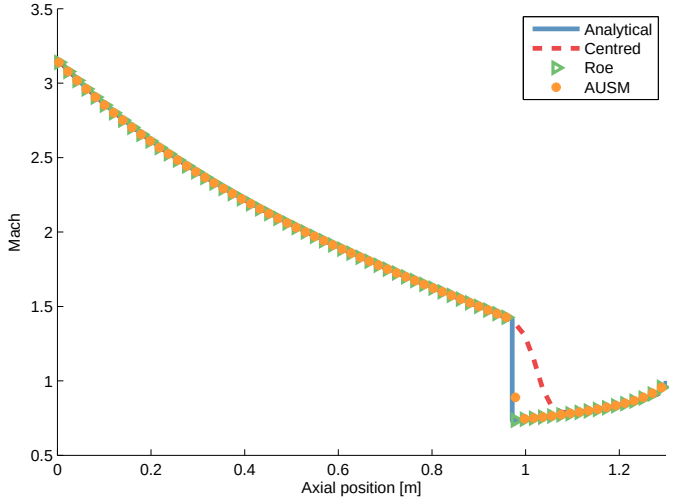

Figure 4: Fanno flow: supersonic test case with shock comparison of centred, Roe and AUSM scheme

	Subsonic	Supersonic
Initial Conditions		
pressure [Pa]	451622	50812
temperature [K]	657.7	417
velocity [m/s]	298.1	1283
length [m]	1.3	1.3/1.1
Inlet Conditions		
pressure [Pa]	451622	50812
temperature [K]	657.7	417
velocity [m/s]	298.1	1283
Outlet Conditions		
pressure [Pa]	200000	200000
temperature [K]	657.7	417

Table 2: Initial and boundary conditions for Fanno flow: subsonic and supersonic test cases

tected for the supersonic cases in both components. It has to be noticed that the shock predicted by the AUSM scheme has a slightly more smeared profile, indicating that this scheme can be more dissipative than the Roe scheme.

3.1.2 Unsteady test case: water hammer

The pipe component is now tested on a phenomena interesting real feed lines of a propulsion system. The water hammer here presented is typical of a satellite propulsion system start-up sequence, when, after a fast opening of the valves placed downstream the tanks, all the propulsion circuit is pressurised. The overpressure arising from the pressurisation procedure is of particular importance in the dimensioning of the propulsion subsystems, such as valves, lines, filters and other elements that may be integrated in the system. This test is here proposed because it has a strongly unsteady behaviour and is characterised by a fluid structure that is typically two-phase.

Input Data	Pipe_gas
number of nodes	20
length [m]	0.67
outer diameter [m]	0.011
thickness [m]	0.001
material	Titanium
initial stagnation pressure [Pa]	$20e^{5}$
initial stagnation temperature[K]	283.15
non-condensable gas fraction	0
fluid	water
	Junction
valve area [m^2]	$7.854e^{-5}$
Forward/Backward loss coefficient	3
valve position	open

Table 3: ESPSS input data for the schematic in Fig.6 [11, 10]

Experiments for the set-up shown in Fig. 5 have been run with water [9]. The set-up for the experiment within EcosimPro

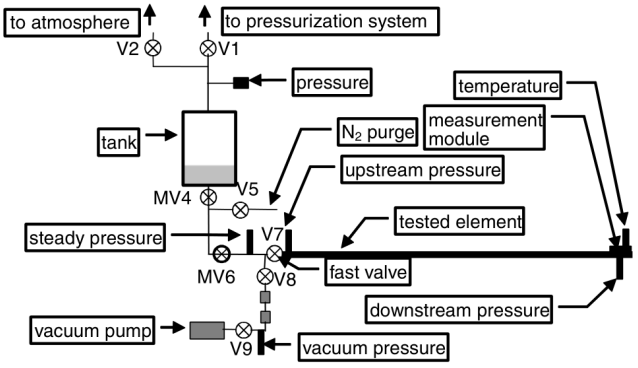

Figure 5: Experimental set-up for water hammer test case [10]

is based on the test case reported in the "Software Verification and Validation Plan document"(STP) [11], provided with the software and referenced to the experimental work reported in [10], [9].

The simulation is characterised by the schematic reported in Fig. 6 where all the main components are explained in Table Tables 3 and 4

Starting from the initial conditions, the fast opening valve is quickly released and set in a full open position, 25 ms after the simulation starting time. Left boundary conditions of stagnation pressure and temperature "BC_sx" are set at the "Pipe_liq" values, whereas the right boundary values are set to ambient conditions, being not effective on the simulation because of the closed position of the valve "D_end". The liquid stored in the system upstream the valve "V7" suddenly fills the rest of the system, approaching the dead end. This causes high pressure peaks in the end of the "Pipe_gas". The

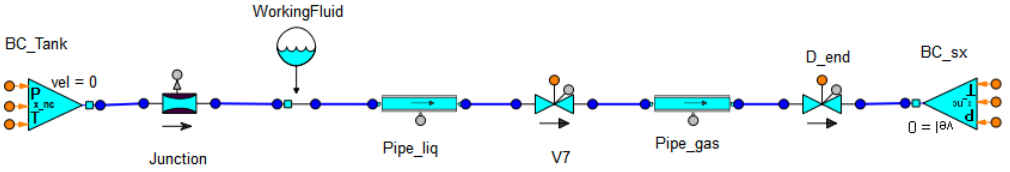

Figure 6: Water hammer test case EcosimPro schematic

Input Data	Pipe_liq
number of nodes	50
length [m]	2.00
outer diameter [m]	0.00594
thickness [m]	0.00041
material	Titanium
initial stagnation pressure [Pa]	$0.1e^5$
initial stagnation temperature[K]	283.15
non-condensable gas fraction	0
fluid	water
	V7
valve area [m^2]	$2.40018e^5$
forward/backward loss coefficient	3
valve position	linear

Table 4: ESPSS input data for the schematic in Fig.6 [11, 10]

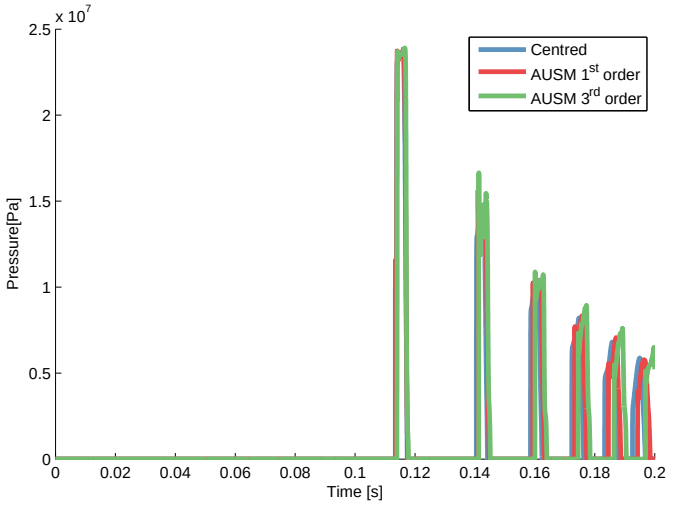

(a) Time evolution up to 0.2 s

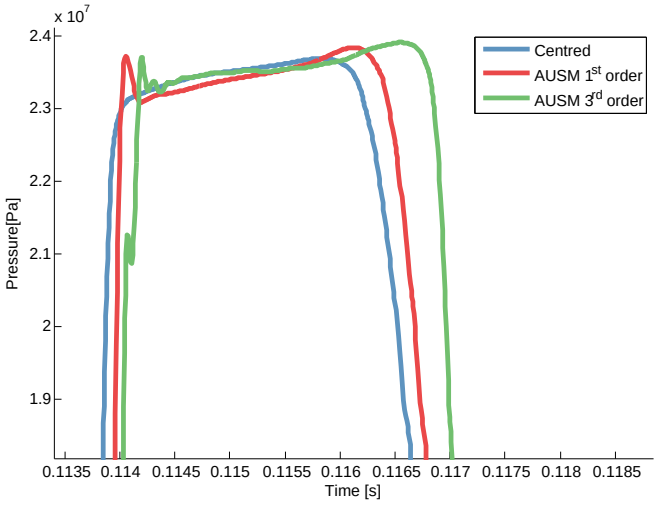

(b) Close-up on first pressure peak

Figure 7: Water hammer test case with water: pressure comparison for different scheme. Mesh size: 50 nodes.

amplitude and the frequency of the peaks are highly influenced by the initial conditions of the "Pipe_gas" itself. In the present case the pipe is filled with a saturated vapour of the liquid stored in the system upstream the valve "V7", that is set to be water. In the next section the results for both liquids will be compared for different solvers in order to show the behaviour of the implementation when compared with the numerical schemes presently available in ESPSS.

In Fig. 7- 8 the results obtained with the centred, AUSM for both first and third order are presented whereas the Roe scheme fails to converge in all the test cases. The pressure evolution shows the successive pressure peak cycles due to the abrupt stop of the liquid front onto the dead end of the pipe. The experimental value of 28.9 MPa [9] is always underestimated. In order to make the needed comparisons we consider as predicted pressure peak the value registered at the end of each plateau [10] characterising each of the first pressure peaks, as shown in Fig. 7(b). The first spike before the plateau is here considered as associated to numerical effects of the schemes. The higher pressure peak is registered by the third order accurate AUSM scheme. Furthermore, the position of the peaks remain almost unchanged with both AUSM and centred scheme. No experimental evidences were measured for the both mixture temperature and vapour volume fraction, here reported respectively in Fig. 8(a) and Fig. 8(b). The higher temperature value is computed by the centred scheme, while the AUSM scheme predicts the values that are smaller of both the other schemes. The vapour volume fraction gives informations about position of the liquid front, decreasing from 1 to 0 when the vapour is compressed and the tube is filled by the liquid column. It must be noted that in this case all the schemes give similar information with respect to the first vapour volume fraction drop, located at

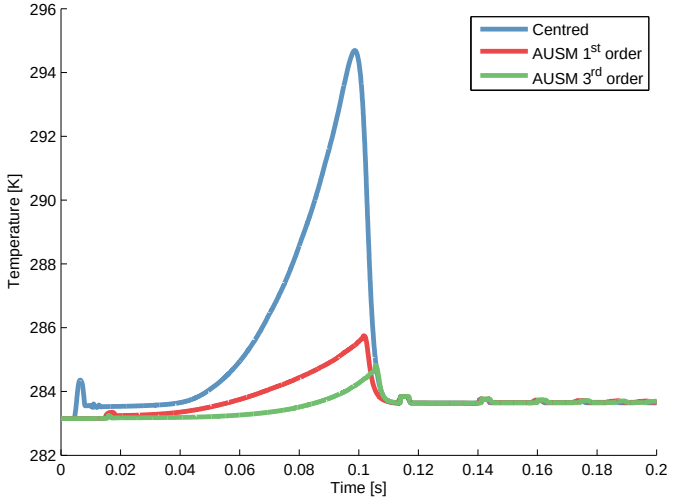

(a) mixture temperature

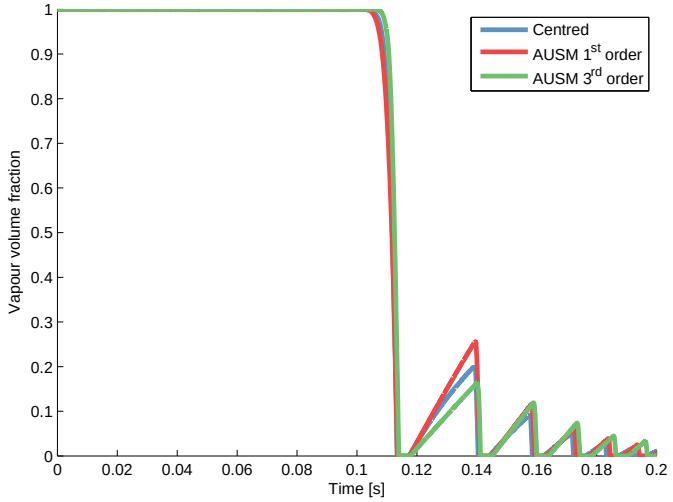

(b) vapour volume fraction comparison

Figure 8: Water hammer test case with water: property comparisons up to 0.2s. Mesh size: 50 nodes.

$t \approx 0.11$ s. Due to this results, it seems that AUSM scheme with a first order reconstruction is able to give results that are in line with a higher order reconstruction, thus allowing to save computational time while preserving a certain accuracy in the reconstruction of the results. It must be underlined that this comparisons have to be evaluated under the limits of the present modelling approach, i.e. the HEM. The phenomena under examination is in fact characterised by a strong two-phase behaviour, where the fluid are far from the homogeneous hypothesis and where the absence of an unsteady friction model can give strong differences when compared with experimental results. For this reason our attention is here focussed on the relative differences among the schemes. In Tables 5 and 6 we report the computational times for all the performed tests. The AUSM scheme proves to be always faster than the Roe scheme for most of the proposed test cases. In the case of Fanno flow supersonic test case the AUSM scheme

	Fanno sub t[s]	Fanno sup t[s]	Fanno sup shock t[s]
Centred	1.491	2.024	2.24
Roe 3^{rd} order	9.284	13.05	40.39
AUSM 3^{rd} order	8.267	49.67	53.3

Table 5: Computational time comparison Fanno test cases: donor-cell, Roe and AUSM scheme

	Water hammer t[s]
Centred	4.253
Roe 1^{st} order	NOK
AUSM 1^{st} order	4.872
Roe 3^{rd} order	NOK
AUSM 3^{rd} order	5.447

Table 6: Computational time comparison water hammer test cases: donor-cell, Roe and AUSM scheme

leads to longer computational times, especially in the test case without a shock inside the tube. This behaviour could be related to the initial conditions shared by both the supersonic test cases. Nevertheless, it must be pointed out that the Fanno test case aims at reaching a known steady state starting from fictitious initial conditions and that when applied to real system configurations (e.g. water hammer test case) the AUSM scheme proves to be more robust than the Roe scheme and to give computational times in line with the centred scheme.

3.2 Combustion chamber component

The AUSM implementation for the thrust chamber is now tested on a gas generator engine cycle. The AUSM scheme in the component is used to model the combustion chamber up to the throat section, whereas the diverging section is modelled by means of steady state correlations [1]. The model here presented is the one proposed in the STP [11] document which is based on fictitious input data values, with the aim of proving ESPSS libraries capabilities in modelling gas generator engine cycles. Being a generic engine no informations where available for the turbopump assembly, therefore generalised performance maps for both pumps and turbines have been used. The main engine data are reported in Table 7 and the simulation here proposed starts at 1.5 s.

The AUSM scheme proves to be efficient and robust by giving a smooth profile in both start-up and shut-down transients. The computational time in Table 8 show that the increased level of complexity achieved with the AUSM scheme comes at the price of longer computational times. It has to be noted that the Roe scheme has never been implemented in the component and that the AUSM scheme is the only option available to properly model the unsteady evolution of 1D fluid-dynamic

Propellants thrust kN	Liq. Oxygen	Liq. Hydrogen 553
Pre-burner		
mixture ratio chamber pressure [Pa]		1 $105e^5$
Combustion chamber		
mixture ratio chamber pressure [Pa]		7.5 $70.5e^5$
Pump		
discharge pressure [Pa] speed [rad/s]	$140.5e^5$ 1337	$147.5e^5$ 3299
Tank		
pressure [Pa] temperature [K]	$7e^5$ 92	$3.5e^5$ 22

Table 7: Gas generator engine main parameters at setady state

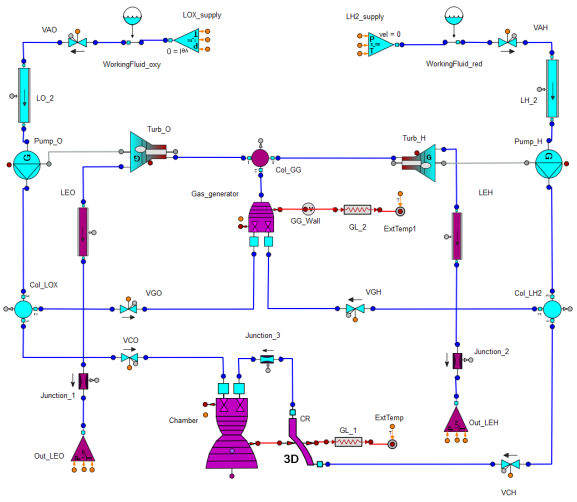

Figure 9: Gas generator test case: EcosimPro schematic

	Gas generator t[s]
Centred	358.5
Roe 1^{st} order	n/a
AUSM 1^{st} order	685.4
Roe 3^{rd} order	n/a
AUSM 3^{rd} order	675.4

Table 8: Computational time comparison gas generator test cases: donor-cell and AUSM scheme

structures inside the thrust chamber.

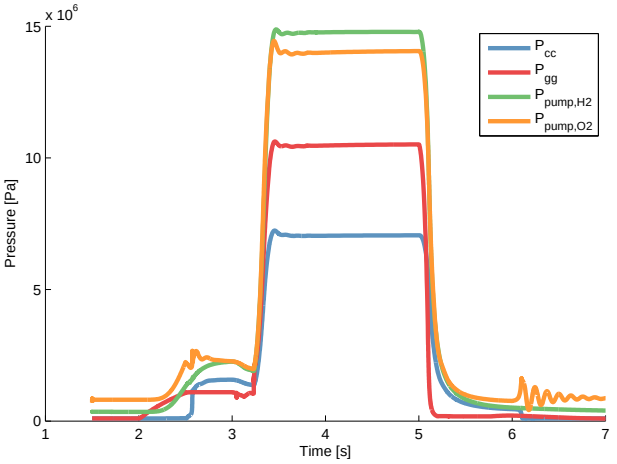

Figure 10: Gas generator test case: combustion chamber, pre-bruner and pumps discharge pressures

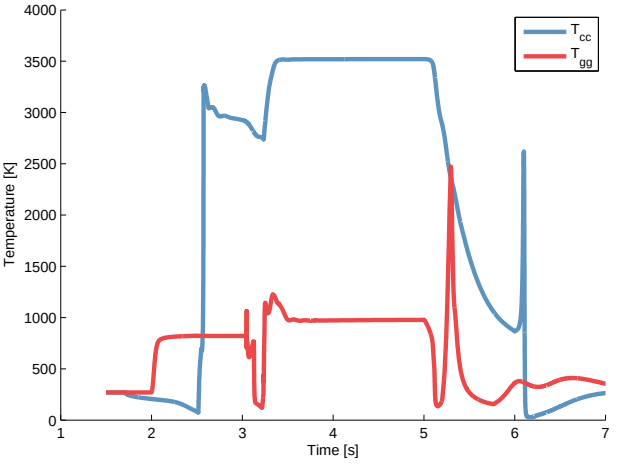

Figure 11: Gas generator test case: combustion chamber and pre-bruner temperatures

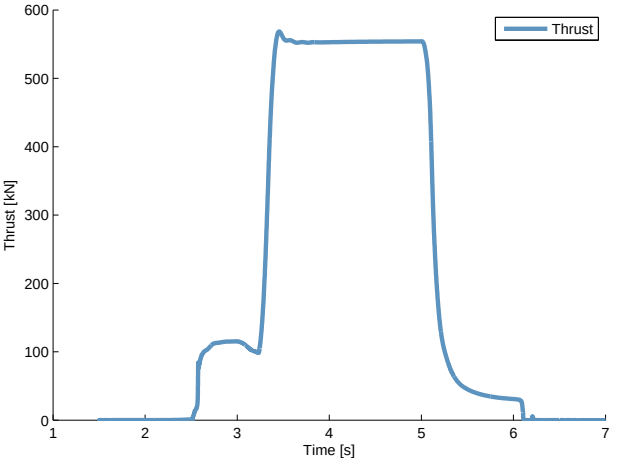

Figure 12: Gas generator test case: Thrust

4 Conclusions

The AUSM scheme has been implemented and validated in several components of the ESPSS library. The extension of the scheme to the HEM required particular attention to the definition of the interface speed of sound. The solution here adopted guarantees a robust behaviour over a broad range of operational configurations, making the scheme an appealing alternative. It proves to converge in all the test cases here reported, even in those where the Roe scheme fails. In particular, strong transient phenomena like water hammer, where intense fluid dynamic structures characterise the flow evolution, can now be modelled with computational times comparable to those of the centred scheme. The relatively simple formulation of the scheme enables its implementation also in the multi-species code modelling the combustion chamber components (i.e. rocket engines and ramjet). The AUSM proves to behave robustly, thus enabling for more accurate computations of the unsteady flow field inside the combustion chambers. However, the user must be aware of the higher computational cost that may be faced when using the AUSM instead of a simple centred scheme when modelling the combustion chamber component, especially when modelling a complete engine.

Acknowledgements

This work has been conducted in the framework of the ESA-TRP on "Multi-Phase Flow Modelling" N.4000111093/14/NL/PA funded by the European Space Agency.

REFERENCES

[1] EA Internacional, *EcosimPro user manual 3.0.6*, EA Internacional, 2015.

[2] Liou, M., "A sequel to AUSM, Part II: AUSM$^+$-up for all speeds," *Journal of Computational Physics*, Vol. 214, No. 1, 2006, pp. 137 – 170.

[3] Liou, M. and Edwards, J. R., "Numerical speed of sound and its application to schemes for all speeds," Tech. rep., NASA, Glenn Research Center, Cleveland, Ohio, 1999.

[4] Edwards, J. R., Franklin, R. K., and Liou, M., "Low-diffusion flux-splitting methods for real fluid flows with phase transitions," *AIAA journal*, Vol. 38, No. 9, 2000, pp. 1624–1633.

[5] Liou, M., "A Sequel to AUSM: AUSM$^+$," *Journal of Computational Physics*, Vol. 129, No. 2, 1996, pp. 364 – 382.

[6] Wada, Y. and Liou, M., "An Accurate and Robust Flux Splitting Scheme for Shock and Contact Discontinuities," *SIAM J. Sci. Comput.*, Vol. 18, No. 3, May 1997, pp. 633–657.

[7] Edwards, J. and Liou, M., "Low-Diffusion Flux-Splitting Methods for Flows at All Speeds," *AIAA Journal*, Vol. 36, 1998, pp. 1610–1617.

[8] Kim, K. H., Kim, C., and Rho, O., "Methods for the Accurate Computations of Hypersonic Flows," *Journal of Computational Physics*, Vol. 174, 2001, pp. 38–80.

[9] Gibek, I. and Maisonneuve, Y., "Waterhammer Tests with Real Propellants," *AIAA/SAE/ASME/ASEE 41st Joint Propulsion Conference and Exhibit*, No. AIAA 2005-4081, 2005.

[10] Lecourt, R. and Steelant, J., "Experimental investigation of waterhammer in simplified feed lines of satellite propulsion systems," *Journal of Propulsion and Power*, Vol. 23, No. 6, 2007, pp. 1214–1224.

[11] Empresarios Agrupados, Astrium, Cenaero, KopooS, Von Karman Institute, and Sapienza University of Rome, "ESPSS: Software Verification and Validation Plan 3.1.0," 2015.